Journal of Power Sources 185 (2008) 946–951

Contents lists available at ScienceDirect

Journal of Power Sources

journal homepage: www.elsevier.com/locate/jpowsour

Short communication

Evaluation of nano-structured $Ir_{0.5}Mn_{0.5}O_2$ as a potential cathode for intermediate temperature solid oxide fuel cell

Bangwu Liu [a], Yousong Gu [a], Lingcai Kong [a], Yue Zhang [a,b,*]

[a] Department of Materials Physics, University of Science and Technology Beijing, Beijing 100083, People's Republic of China
[b] Key Laboratory of New Energy Materials and Technologies, University of Science and Technology Beijing, Beijing 100083, People's Republic of China

ARTICLE INFO

Article history:
Received 1 July 2008
Accepted 7 July 2008
Available online 30 July 2008

Keywords:
$Ir_{0.5}Mn_{0.5}O_2$
Cathode
SOFC
AC impedance

ABSTRACT

A novel $Ir_{0.5}Mn_{0.5}O_2$ cathode has been synthesized by thermal decomposition of mixed H_2IrCl_6 and $Mn(NO_3)_2$ water solution. The $Ir_{0.5}Mn_{0.5}O_2$ cathode has been characterized by XRD, field emission SEM (FESEM) and AC impedance spectroscopy. XRD result shows that rutile-structured $Ir_{0.5}Mn_{0.5}O_2$ phase is formed by thermal decomposition of mixed H_2IrCl_6 and $Mn(NO_3)_2$ water solution. FESEM micrographs show that a porous structure with well-necked particles forms in the cathode after sintering at 1000 °C. The average grain size is between 20 and 30 nm. Two depressed arcs appear in the medium-frequency and low-frequency region, indicating that there are at least two different processes in the cathode reaction: charge transfer and molecular oxygen dissociation followed by surface diffusion. The minimum area specific resistance (ASR) is 0.67 Ω cm^2 at 800 °C. The activation energy for the total oxygen reduction reaction is 93.7 kJ mol^{-1}. The maximum power densities of the $Ir_{0.5}Mn_{0.5}O_2$/LSGM/Pt cell are 43.2 and 80.7 mW cm^{-2} at 600 and 700 °C, respectively.

1. Introduction

Intermediate temperature solid oxide fuel cell (ITSOFC) (operating temperature: 500–800 °C) has attracted much attention in recent years [1]. Low operating temperature will allow the selection of material from a wide range, reduce the interactions between the electrodes and the electrolyte, and promote the commercialization of SOFC [2]. However, the popular $La_{1-x}Sr_xMnO_3$ (LSM) cathode is not a good choice in the intermediate temperature range since the overpotential increases dramatically as the operating temperature decreases [3]. One of the most important objects in the development of SOFC is to improve the electrode's performance, especially for the cathode. The requirements for the cathode material are as follows: adequate porosity for oxygen supply, good catalytic property and conductivity for oxygen dissociation and transportation, compatibility with the electrolyte and long term stability [4]. IrO_2 is a probable candidate for cathode because of its high catalytic activity for reduction of oxygen [5]. It also has a high conductivity comparable with metals and a high chemical inertness. Torres-Huerta [5] prepared IrO_2/YSZ nano-composite cathode and found that IrO_2 displayed superior electrochemical properties for a cathode. However, IrO_2 is very expansive. In an effort to look for a cheap cathode material, MnO_2 is found to be a kind of green material with an excellent electro-catalytic activity [6]. Hibino et al. [7] have found that the addition of MnO_2 to the LSM cathode could improve the open circuit voltage (OCV) and the peak power density. Therefore, it is possible to reduce the cost by using MnO_2 doped IrO_2 as a potential cathode for ITSOFC.

In this paper, $Ir_{0.5}Mn_{0.5}O_2$ was studied as a potential cathode material by focusing on the electrochemical performance of $Ir_{0.5}Mn_{0.5}O_2$ cathode on $La_{0.9}Sr_{0.1}Ga_{0.8}Mg_{0.2}O_{3-\delta}$ electrolyte evaluated by AC impedance spectroscopy.

2. Experimental

2.1. Cell fabrication

The $La_{0.9}Sr_{0.1}Ga_{0.8}Mg_{0.2}O_{3-\delta}$ (LSGM) powders were synthesized by glycine–nitrate combustion method. The initial materials were Ga_2O_3 (99.999%), $La(NO_3)_3{\cdot}6H_2O$ (analytical reagent grade), $Mg(NO_3)_2$ (analytical reagent grade), $Sr(NO_3)_2$ (analytical reagent grade), and glycine (H_2NCH_2COOH, analytical reagent grade). The detailed preparation procedure was described elsewhere [8]. The as-prepared LSGM powders were calcined at 1000 °C for 2 h to decompose residual reactants. The calcined LSGM powders were sintered as an electrolyte pellet at 1250 °C under a pressure of

* Corresponding author. Tel.: +86 10 62333113; fax: +86 10 62332281.
E-mail address: yuezhang@ustb.edu.cn (Y. Zhang).

0378-7753/$ – see front matter © 2008 Elsevier B.V. All rights reserved.
doi:10.1016/j.jpowsour.2008.07.059

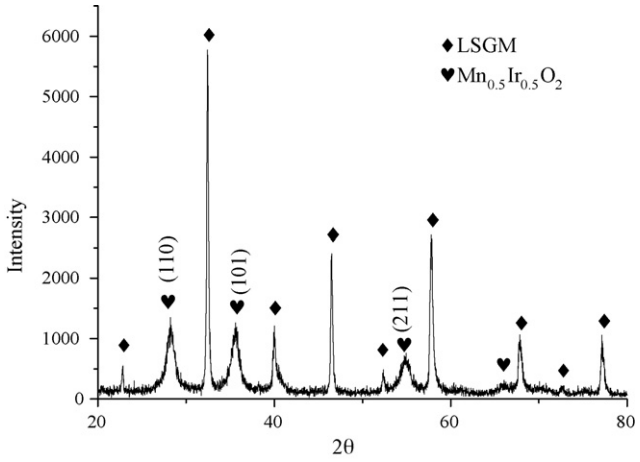

Fig. 1. XRD pattern of $Ir_{0.5}Mn_{0.5}O_2$ cathode on LSGM electrolyte after sintering at 1000 °C.

40 MPa by spark plasma sintering (SPS). Both sides of the pellet were roughed with 240# SiC grit paper and then sonicated for 10 min. $Ir_{0.5}Mn_{0.5}O_2$ was prepared by thermal decomposition of mixed H_2IrCl_6 (J&K Chemical Ltd.) and $Mn(NO_3)_2$ (J&K Chemical Ltd.) water solution. The total metal ion concentration of the precursor was kept around 0.2 M. The precursor solution was painted onto the both sides of the LSGM pellet by a brush. The cell was first dried at 100 °C for 10 min, and then heated at 450 °C for 10 min to decompose the precursor. This procedure was repeated for 2–3 cycles. Finally, the cell was sintered at 1000 °C for 2 h. A symmetrical cell with cathode films of about 0.29 cm^2 was obtained. In order to obtain the output performance, a $Ir_{0.5}Mn_{0.5}O_2$/LSGM/Pt single cell was prepared with $Ir_{0.5}Mn_{0.5}O_2$ cathode one side of the LSGM pellet and Pt anode on the other side. Pt anode was prepared by brushing Pt paste on one side of the pellet and sintering at 850 °C for 1 h.

2.2. Characterization

XRD using Cu Kα radiation on a Rigaku Dmax-RB X-ray diffractometer was carried on to study the phase formation. Morphology of the cathode was observed in a SUPRA-55 FESEM with an accelerating voltage of 10 kV. TEM image and selected area electron diffraction (SAED) measurements were performed using a transmission electron microscope (JEM-1OOCX). Two Pt plates were used as current collectors attached to two Pt wires for symmetrical cell experiments. AC impedance measurements were performed using a Solartron 1255 HF frequency response analyzer coupled with an EG&G PARC 273 potentiostat under different temperature and oxygen partial pressure. The oxygen partial pressure varied from 1, 0.21, 0.1 to 0.01 atm. The frequency ranged from 100 KHz to 0.01 Hz. The measurements were carried out under open circuit potential with a perturbation amplitude of 20 mV. The impedance spectra were analyzed in terms of equivalent circuits with the ZSIMWIN software. *I–V* polarization curves were measured using a Keithley 2410 source meter in the four terminal configuration. The $Ir_{0.5}Mn_{0.5}O_2$/LSGM/Pt single cell was sealed onto a quartz tube reactor with the cathode side exposed to ambient air. Pure hydrogen was fed into the anode chamber as fuel.

3. Results and discussion

3.1. Crystal structure analysis

Fig. 1 presents the XRD pattern of cathode on LSGM electrolyte after sintering at 1000 °C for 2 h. The rutile-structured $Ir_{0.5}Mn_{0.5}O_2$ phase can be obtained from thermal decomposition of mixed H_2IrCl_6 and $Mn(NO_3)_2$. A comparison with JCPDS 88-0288 and 24-0735 for IrO_2 and MnO_2 are show in Table 1. It can be see that the peak position is between the peaks expected for the IrO_2 and MnO_2 tetragonal structure, which suggests that the mixed oxide system forms a solid solution of IrO_2 and MnO_2 with the rutile-type structure. This result is in line with the Hume–Rothery conditions because both oxides have a tetragonal structure and similar valence.

Table 1
The XRD peak positions and d spacing of $Ir_{0.5}Mn_{0.5}O_2$ compared with the JCPDS data.

Peak index	$Ir_{0.5}Mn_{0.5}O_2$		JCPDS88-0288 (IrO_2)		JCPDS24-0735 (MnO_2)	
	2θ (°)	d (Å)	2θ (°)	d (Å)	2θ (°)	d (Å)
(1 1 0)	28.125	3.1702	27.987	3.1855	28.680	3.1100
(1 0 1)	35.611	2.5190	34.656	2.5862	37.328	2.4070
(2 1 1)	54.761	1.6749	53.935	1.6986	56.652	1.6234

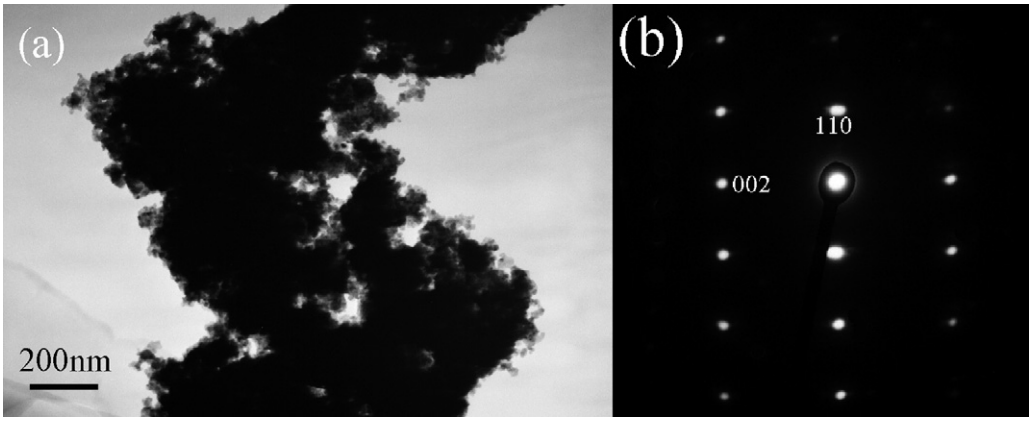

Fig. 2. (a) TEM image and (b) SAED pattern of $Ir_{0.5}Mn_{0.5}O_2$ clusters.

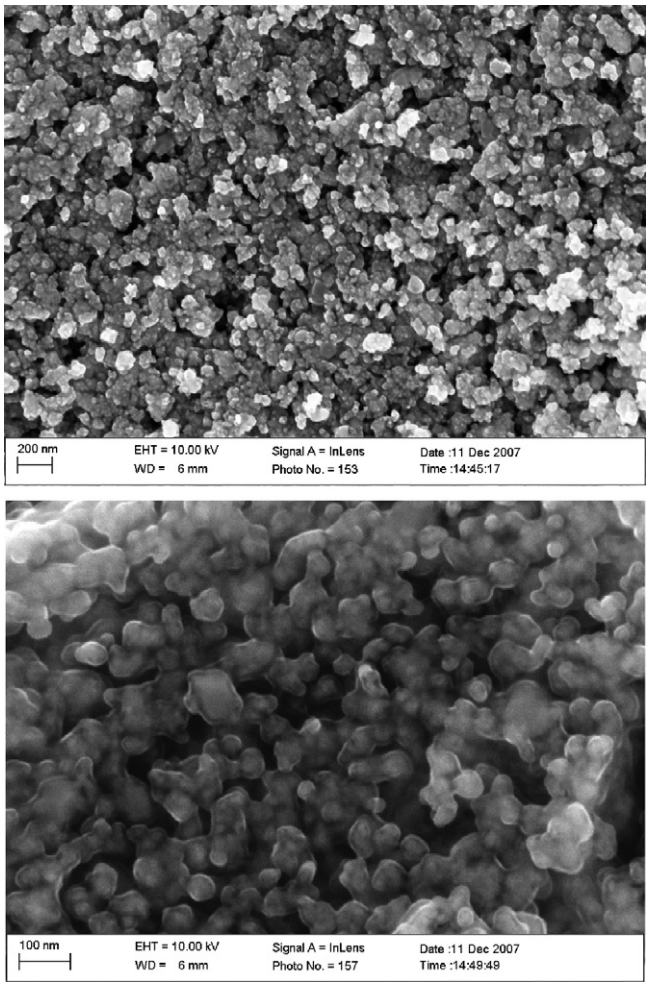

Fig. 3. FESEM micrographs of the $Ir_{0.5}Mn_{0.5}O_2$ cathode sintered at 1000 °C.

Grupioni et al. [9] have investigated 30%IrO_2–70%MnO_2 system and got a similar conclusion. The big FWHM of the XRD peaks of $Ir_{0.5}Mn_{0.5}O_2$ suggests a fine grain size of $Ir_{0.5}Mn_{0.5}O_2$.

Fig. 2 shows the TEM micrograph and the SAED of the mixed oxide. It is clear that a tetragonal rutile-structure was formed, in agreement with the XRD pattern.

3.2. Morphology characteristics

Fig. 3 shows surface micrographs of the $Ir_{0.5}Mn_{0.5}O_2$ cathode sintering at 1000 °C for 2 h. It seems that the particles are well connected to each other after sintering. The cathode presents a well-bonded porous network which is composed of many well-dispersed and connected $Ir_{0.5}Mn_{0.5}O_2$ grains and uniform pores. The high porosity of the cathode and the good connection between the grains can not only enlarge the reactive areas, but also maintain high electron paths through the cathode framework. The average grain size is 20–30 nm. As the particle size decreases to nano-scale, the area of triple phase boundaries (TPB), where reduction of oxygen occurs, is dramatically increased, and the O_2 reduction reaction is enhanced [10,11].

3.3. Electrochemical performances

Fig. 4 shows the output performances of the $Ir_{0.5}Mn_{0.5}O_2$/LSGM/Pt single cell using pure H_2 as fuel at 600 and 700 °C, respectively. The power density of the cell increases with operating temperature. The maximum power densities of the cell are 43.2 and 80.7 mW cm^{-2} at 600 and 700 °C, respectively.

The AC impedance spectra for the symmetrical cell measured at temperatures between 450 and 800 °C in air are shown in Fig. 5. From the spectra, a high frequency induction tail can be seen, which is due to the device and the connect wires. By fitting the spectra, the two depressed arcs appear at medium-frequency and low-frequency, implying that there are at least two different processes in the cathode reaction. All the spectra data can be well fitted by the equivalent circuit of the type $R_o(R_mQ_m)(R_lQ_l)$ shown in Fig. 5, where R_o is the combination of electrolyte resistance, electrode ohmic resistance, wire resistance and contact resistance between cell and the Pt plates. Q is a constant phase element representing time-dependent capacitive elements. The first component (R_mQ_m) appears as a depressed arc at medium-frequency and the second one (R_lQ_l) appears a depressed arc at low-frequency region. Q represents a non-ideal capacitor and the associated n parameter indicates the Q's similarity to a true capacitor. The constant phase element (Q) can be transformed into capacitances using the equation: $C = (RQ)^{1/n}/R$ [12]. All the data are well fitted by the equivalent circuit and the errors estimated by the program are within 10%.

Arrehenius plots of R_m and R_l can be seen in Fig. 6. Both R_m and R_l decrease rapidly with temperature. The activation energy for the arc in the medium-frequency region is 99.86 kJ mol^{-1} and the capacitance calculated from the fitting results is on the order of 10^{-4} F cm^{-2}. So the medium-frequency arc can be related to a charge transfer process. The activation energy for the second arc is 88.6 kJ mol^{-1}, indicating a non-gas diffusion process. The capacitance calculated from the fitting results is in the range 0.05–0.2 F cm^{-2}, which is too large to be associated with a double layer capacitance. Escudero et al. [13] have studied oxygen reduction reaction on La_2NiO_4 cathodes and found that the process in the low-frequency region is assigned to molecular oxygen dissociation phenomena. Our data are similar with theirs, and this arc can be associated as molecular oxygen dissociation. From Fig. 5, it can be seen that the medium-frequency arc is larger than the low-frequency arc, indicating charge transfer process probably limits the cathode reaction.

In order to further understand the oxygen reduction mechanism on the cathode, impedance measurements were done as a function of oxygen partial pressure. The P_{O_2} dependences of the polarization resistance (R_p) in the medium-frequency and low-frequency arcs determined from the $\log(1/R_m) - \log P_{O_2}$ and $\log(1/R_l) - \log P_{O_2}$ plots at different temperatures are shown in Figs. 7 and 8. The

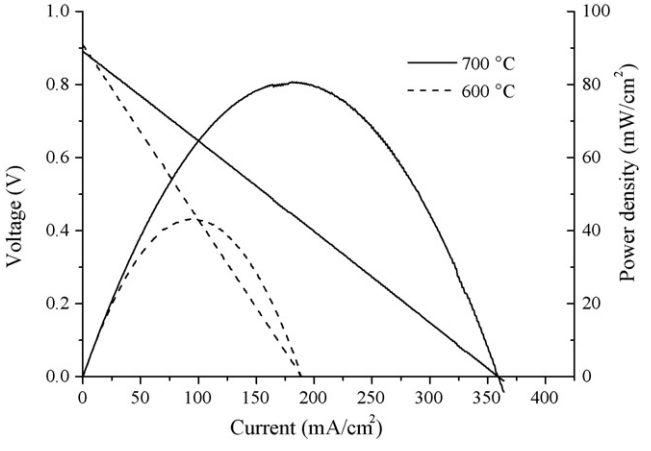

Fig. 4. The output performances of the $Ir_{0.5}Mn_{0.5}O_2$/LSGM/Pt cell at 600 and 700 °C.

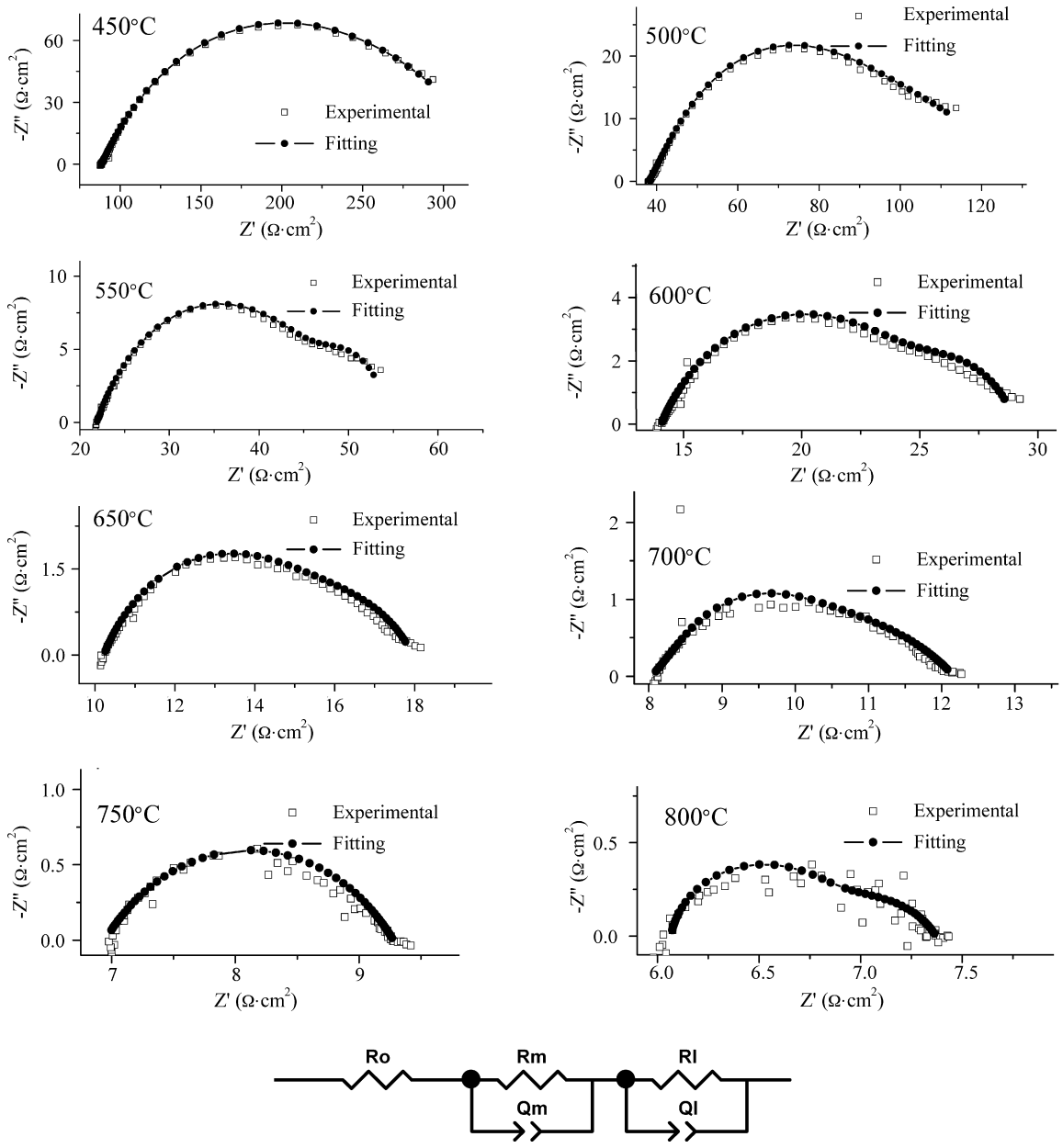

Fig. 5. The AC impedance spectra for the symmetrical cell and equivalent circuit.

polarization resistance of the cathode varies with the oxygen partial pressure according to the following equation [14]:

$$R_p^{-1} \propto P_{O_2}^{x}$$

- where x is the reaction order which provides an insight into the rate-limiting step of the oxygen reduction reaction on the electrodes. For metal and metal oxide cathodes on solid electrolytes,
- $x = 0.25$, the charge transfer reaction at the triple phase boundary is the rate-determining process;
- $x = 0.5$, the surface diffusion of the dissociative adsorbed oxygen at the triple phase boundaries is involved in the rate-determining step;
- $x = 1$, gaseous diffusion of oxygen molecules in the porous structure is the rate-determining process.

The x values determined from the slope at different temperatures in Figs. 7 and 8 are listed in Table 2. It can be seen in Table 2, $x = 0.25$ for R_m is observed, indicating that the oxygen reduction reaction in the medium-frequency is a charge transfer process. The x values for the low-frequency arc ranged between 0.52 and 0.59. Due to the values of the activation energies and capacitances, we suggest the oxygen reduction reaction process at low-frequency is molecular oxygen dissociation followed by the surface diffusion.

It is widely established that the performance of ITSOFC is strongly dependent on cathode area specific resistance (ASR), which must be minimized to obtain high ITSOFC power densities

Table 2
Reaction orders under different temperatures.

T (°C)	x for R_m	x for R_l
600	0.242	0.518
700	0.256	0.576
800	0.266	0.591

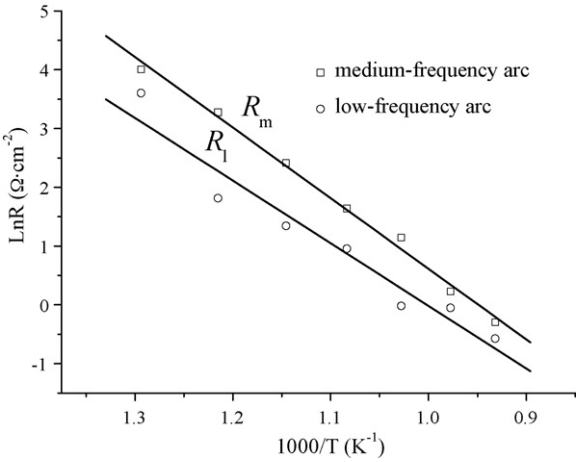

Fig. 6. Arrehenius plots of R_m and R_l as a function of the temperature in air.

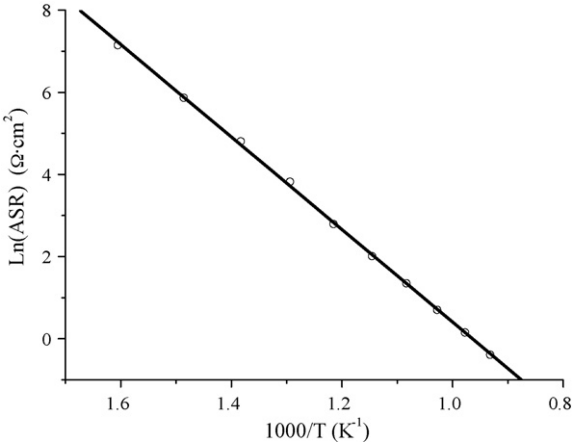

Fig. 9. Arrehenius plot of ASR as a function of the temperature.

[15,16]. For a symmetrical cell, the ASR can be calculated according to the following equation: ASR = (R_p*A)/2, where R_p is the sum of the resistances of each process ($R_p = R_m + R_l$), A is the electrode area, and the factor 2 is due to the fact that each cell has two (roughly identical) electrodes. Arrehenius plot of ASR as a function of temperature in air is shown in Fig. 9. As expected, the ASR of $Ir_{0.5}Mn_{0.5}O_2$/LSGM interface decreases rapidly with increasing temperature. The minimum ASR is 0.67 Ω cm^2 at 800 °C. The ASR of the $Ir_{0.5}Mn_{0.5}O_2$ cathode on LSGM electrolyte is lower than that of the IrO_2/YSZ composite cathode on YSZ electrolyte reported by Torres-Huerta [5]. The activation energy for the total oxygen reduction reaction is 93.7 kJ mol^{-1}, which is slightly lower than that of LSM cathode (about 100 kJ mol^{-1}) [17].

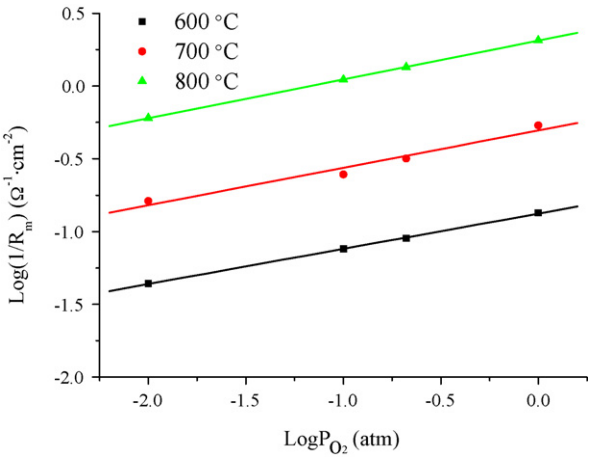

Fig. 7. Dependence of reciprocal R_m on oxygen partial pressure at 600, 700, and 800 °C.

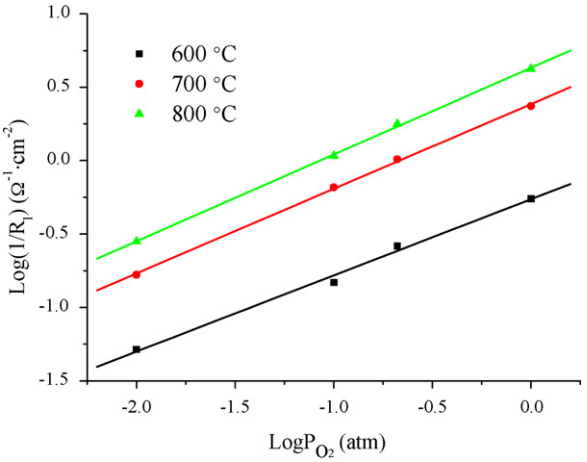

Fig. 8. Dependence of reciprocal R_l on oxygen partial pressure at 600, 700, and 800 °C.

The ASR can be decreased in two ways: increasing the triple phase boundaries by control of the microstructure combined with a contiguous ionic conducting phase, which allows electrochemical reactions to occur within the cathode; improving the kinetics of oxygen exchange and diffusion. It should be noted that IrO_2 is a favorable catalyst for oxygen dissociation reaction, which will certainly improve the catalytic activity for the oxygen reduction at the cathode. Therefore, the ASR of $Ir_{0.5}Mn_{0.5}O_2$ cathode could be further decreased by increasing the triple phase boundaries by control of the microstructure combined with a contiguous ionic conducting phase. The above results indicate that the $Ir_{0.5}Mn_{0.5}O_2$ materials synthesized in this work may offer an efficient and competitive performance as cathode material for ITSOFC. However, further studies will be required in order to determine the stability of the cathode and improve its performance in the solid oxide fuel cell.

4. Conclusions

A novel $Ir_{0.5}Mn_{0.5}O_2$ cathode has been synthesized by thermal decomposition of a mixed H_2IrCl_6 and $Mn(NO_3)_2$ water solution. The $IrO_2 + MnO_2$ cathodes have rutile structure and do not react with LSGM electrolyte. After sintering at 1000 °C, cathode is porous with well-necked particles. The average grain size is between 20 and 30 nm. There are two different processes in the cathode reaction: charge transfer and molecular oxygen dissociation followed by surface diffusion. The minimum ASR is reached 0.67 Ω cm^2 at 800 °C and the activation energy for the total oxygen reduction reaction is 93.7 kJ mol^{-1}. The maximum power densities of the $Ir_{0.5}Mn_{0.5}O_2$/LSGM/Pt cell are 43.2 and 80.7 mW cm^{-2} at 600 and 700 °C, respectively. The synthesized $Ir_{0.5}Mn_{0.5}O_2$ may offer an efficient and competitive performance as cathode for ITSOFC.

Acknowledgements

This work was supported by National Basic Research Program of China (No. 2007CB936201), the National High Technology Research and Development Program of China (No. 2006AA03Z351), and the

Major Project of International Cooperation and Exchanges (Nos. 50620120439, 2006DFB51000).

References

[1] Y. Liu, S.W. Zha, M.L. Liu, Adv. Mater. 16 (2004) 256.
[2] Q.L. Liu, K.A. Khor, S.H. Chan, J. Power Sources 161 (2006) 123.
[3] T. Horita, K. Yamaji, M. Ishikawa, N. Sakai, H. Yokokawa, T. Kawada, T. Kato, J. Electrochem. Soc. 145 (1998) A3196.
[4] D.E. Vladikova, Z.B. Stoynov, A. Barbucci, M. Viviani, P. Carpanese, J.A. Kilner, S.J. Skinner, R. Rudkin, Electrochim. Acta 53 (2008) 7491.
[5] A.M. Torres-Huerta, J.R. Vargas-García a, M.A. Domínguez-Crespo, Solid State Ionics 178 (2007) 1608.
[6] Z. Ye, H. Meng, D. Chen, H. Yu, Z. Huan, X. Wang, D. Sun, Solid State Sci. 10 (2008) 346.
[7] T. Hibino, S. Wang, S. Kakimoto, M. Sano, Solid State Ionics 127 (2000) 89.
[8] B. Liu, Y. Zhang, L.M. Zhang, J. Power Sources 175 (2008) 189.
[9] A.A.F. Grupioni, E. Arashiro, T.A.F. Lassali, Electrochim. Acta 48 (2002) 407.
[10] F. Liang, J. Chen, J.L. Cheng, S. Jiang, T. He, J. Pu, J. Li, Electrochem. Commun. 10 (2008) 42.
[11] A. Hagiwara, N. Hobara, K. Takizawa, K. Sato, H. Abe, M. Naito, Solid State Ionics 177 (2006) 2967.
[12] J. Fleig, Solid State Ionics 150 (2002) 181.
[13] M.J. Escudero, A. Aguadero, J.A. Aguadero, L. Daza, J. Electroanal. Chem. 611 (2007) 107.
[14] Y. Takeda, R. Kanno, M. Noda, Y. Tomida, O. Yamamoto, J. Electrochem. Soc. 134 (1987) 2656.
[15] N.P. Brandon, S. Skinner, B.C.H. Steele, Annu. Rev. Mater. Res. 33 (2003) 183.
[16] S. Huang, Z. Zong, C. Peng, J. Power Sources 173 (2007) 415.
[17] A. Barbucci, R. Bozzo, G. Cerisola, P. Costamagna, Electrochim. Acta 47 (2002) 2183.